Inorganic Chemistry

pubs.acs.org/IC

Article

Functional Platinum(II) Complexes with Four-Photon Absorption Activity, Lysosome Specificity, and Precise Cancer Therapy

Qiong Zhang,*,† Shujing Wang,† Yingzhong Zhu, Chengkai Zhang, Hongzhi Cao, Wen Ma, Xiaohe Tian,* Jieying Wu, Hongping Zhou, and Yupeng Tian*

Cite This: *Inorg. Chem.* 2021, 60, 2362−2371

Read Online

ACCESS | Metrics & More | Article Recommendations | Supporting Information

ABSTRACT: Multiphoton materials are in special demand in the field of photodynamic therapy and multiphoton fluorescence imaging. However, rational design methodology for these brands of materials is still nascent. This is despite transition-metal complexes favoring optimized nonlinear-optical (NLO) activity and heavy-atom-effected phosphorescent emission. Here, three four-photon absorption (4PA) platinum(II) complexes (**Pt1**−**Pt3**) are achieved by the incorporation of varied functionalized C^N^C ligands with high yields. **Pt1**−**Pt3** exhibit triplet metal-to-ligand charge-transfer transitions at ∼460 nm, which are verified multiple times by transient absorption spectra, time-dependent density functional theory calculations, and low-temperature emission spectra. Further, **Pt1**−**Pt3** undergo 4PA. Notably, one of the complexes, **Pt2**, has maximum 4PA cross-sectional values of up to 15.2 × 10^{-82} cm^8 s^3 $photon^{-3}$ under excitation of a 1600 nm femtosecond laser (near-IR II window). The 4PA cross sections vary when **Pt2** is binding to lecithin and when it displays its lysosome-specific targeting behavior. On the basis of the excellent 4PA property of **Pt2**, we believe that those 4PA platinum(II) complexes have great potential applications in cancer theranostics.

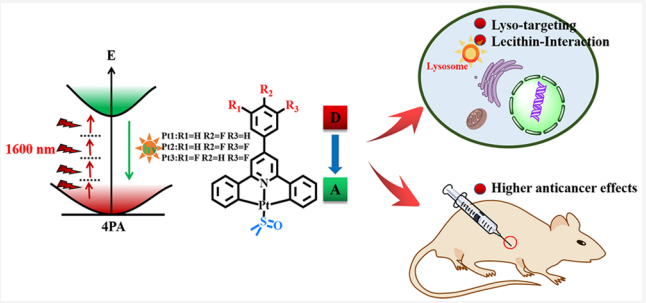

INTRODUCTION

Multiphoton absorption materials include two-photon (2PA), three-photon (3PA), and four-photon (4PA) absorption materials, etc.[1−3] 4PA is defined as being able to absorb four photons simultaneously through virtual states,[4] which is demonstrated by seven-order nonlinear processes.[5,6] 4PA materials can be applied in four-photon pumped-frequency upconversion, 4PA optical limiting, photodynamic therapy, and four-photon fluorescence (4PF) imaging.[7,8] Designing 4PA materials with a rational strategy still poses a great challenge for researchers. In the past, researchers have devoted great effort in the design of effective 4PA materials. The most direct strategy is to extend conjugated systems such as organic materials with D−π−A−π−D, A−π−D−π−A, D−π−D, and D−π−A structures for enhanced electron transfer. However, organic 4PA materials have several disadvantages like unstable structure and complicated synthesis, as stated above.[9−11] Compared to organic materials, transition-metal complexes offer obvious advantages such as plentiful charge transfer, adjustable optical property, and enhanced nonlinear-optical (NLO) activity.[12,13]

In the past, the NLO properties of platinum(II) complexes were always stopping at the 2PA properties. So far, many 2PA-active platinum(II) complexes have been reported.[14−18] However, the excitation wavelengths are slightly narrow, and none of the above could achieve satisfactory 4PA properties. Therefore, the design and synthesis of platinum(II) complexes with 4PA properties in the near-IR (NIR) II region is still a challenge for researchers.

Moreover, it would be better if those platinum(II) complexes promote research interest in cancer theranostics compared to the successful clinical application of the reported platinum anticancer drugs.[19,20]

Inspired by the above backgrounds, we designed and synthesized three D−A-type cyclometalated platinum(II) complexes (**Pt1**−**Pt3**) based on C^N^C ligands, whose structures are confirmed through single-crystal X-ray diffraction. Among them, the crystal structures of F1 and Pt1 have been reported.[21,22] This work mainly studies the structure−activity relationship of the series of complexes of fluorobenzene and tridentate C^N^C ligands of the formate D−A configuration that give rise to intramolecular charge transfer (ICT). Platinum, as a late transition metal, can be coordinated with tridentate C^N^C ligand groups to obtain excellent phosphorescent properties and enhanced ICT. The dimethyl

Received: November 2, 2020
Published: January 25, 2021

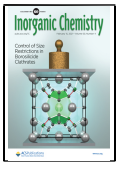

Scheme 1. (a) Chemical Structures for Pt1−Pt3 and (b) Perspective Views of Pt1−Pt3[a]

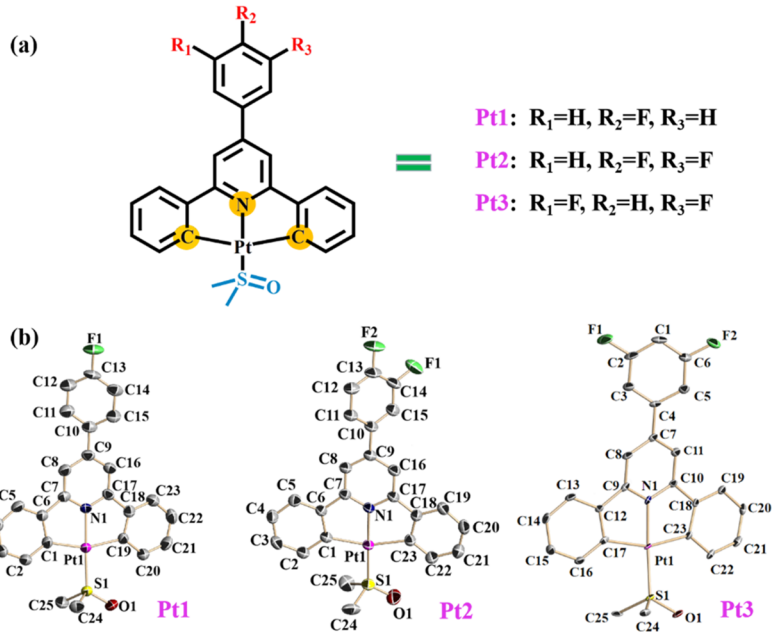

[a]All solvent molecules and hydrogen atoms are omitted for clarity.

sulfoxide (DMSO) group as an auxiliary ligand could afford biocompatibility and could be inserted into DNA, which helps to cut off DNA replication in cancer cells[23−25] (Figure S27). We found that one of the complexes, **Pt2**, exhibits triplet metal-to-ligand charge-transfer (^{3}MLCT) transitions and phosphorescent emission. Strikingly, this complex possesses a large 4PA cross section under 1600 nm femtosecond (fs) laser excitation. Interestingly, live cell evaluation found that this complex exhibits specific colocalization to lysosome in HeLa cells and high toxicity to cancer cells. Careful evaluation of their NLO properties and cell imaging reveal that platinum(II) complexes are capable of specific lysosome targeting in cancer cells because of interaction with lecithin. Thus, our study opens a new avenue for platinum(II) complexes as functional deep-tissue in vivo imaging drugs applied in cancer theranostics. This work is the first report on platinum(II) complexes with 4PA properties.

EXPERIMENTS

1. Synthesis of F1 (Scheme S1). 4-Fluorobenzaldehyde (2.50 g, 20 mmol) and acetophenone (6.10 g, 50 mmol) are dissolved completely in 250 mL of an ethanol solution, and then KOH (5.60 g, 100 mmol) and 150 mL of aqueous ammonia (25%) are added in turn. The mixture is kept at 60 °C for 4 h. Yellow precipitation separates out after cooling and is collected by filtration. A white crystalline solid is obtained from recrystallization using ethanol. Production: 3.90 g. Yield: 60%.

F1. ^{1}H NMR (400 MHz, DMSO-d_6): δ 8.34 (d, J = 7.5 Hz, 4H), 8.20 (s, 2H), 8.14 (dd, J = 8.1 and 5.7 Hz, 2H), 7.56 (t, J = 7.4 Hz, 4H), 7.53 (m, 2H), 7.41 (t, J = 8.7 Hz, 2H). ^{13}C NMR (100 MHz, DMSO-d_6): δ 163.44, 153.61, 152.01, 139.02, 137.91, 130.71, 129.22 127.61, 127.33, 116.03, 115.62. ESI-MS. Calcd for $[M + H]^+$: m/z 326.13. Found: m/z 326.13. FT-IR (KBr, cm^{-1}): 3064, 1606, 1549, 1227, 773.

2. Synthesis of F2 (Scheme S1). A procedure similar to that for **F1** is used, except 3,4-difluorobenzaldehyde (2.84 g, 20 mmol) is used in place of 4-fluorobenzaldehyde. The final product is a white solid. Production: 3.91 g. Yield: 57%.

F2. ^{1}H NMR (400 MHz, DMSO-d_6): δ 8.36 (d, J = 7.3 Hz, 4H), 8.28 (s, 1H), 8.25 (s, 2H), 7.99 (d, J = 8.6 Hz, 1H), 7.65 (s, 1H), 7.56 (t, J = 7.4 Hz, 4H), 7.51 (d, J = 7.1 Hz, 1H), 7.49 (d, J = 7.2 Hz, 1H). ^{13}C NMR (100 MHz, DMSO-d_6): δ 153.61, 152.06, 150.10 139.51, 138.81, 129.22, 127.53, 127.31, 126.10, 118.62, 115.7, 115.11. ESI-MS. Calcd for $[M + H]^+$: m/z 344.12. Found: m/z 344.12. FT-IR (KBr, cm^{-1}): 3063, 1602, 1550, 1278, 787.

3. Synthesis of F3 (Scheme S1). A procedure similar to that for **F1** is used, except 3,5-fluorobenzaldehyde (2.84 g, 20 mmol) is used in place of 4-fluorobenzaldehyde. The final product is a white solid. Production: 4.00 g. Yield: 58%.

F3. ^{1}H NMR (400 MHz, DMSO-d_6): δ 8.38 (d, J = 7.2 Hz, 4H), 8.28 (s, 2H), 7.94 (d, J = 7.1 Hz, 2H), 7.57 (t, J = 7.4 Hz, 4H), 7.54 (m, 2H), 7.39 (dd, J = 12.7 and 5.6 Hz, 1H). ^{13}C NMR (100 MHz, DMSO-d_6): δ 165.03, 153.66, 152.09, 141.81, 139.11, 129.82, 127.63, 127.41, 115.60, 114.72, 105.24. ESI-MS. Calcd for $[M + H]^+$: m/z 344.12. Found: m/z 344.12. FT-IR (KBr, cm^{-1}): 3066, 1647, 1553, 1300, 771.

4. Synthesis of Pt1 (Scheme S1). A total of 0.33 g (1 mmol) of 4-(4-fluorophenyl)-2,6-diphenylpyridine and 0.41 g (1.2 mmol) of K_2PtCl_4 are mixed in 150 mL of acetic acid. The suspension liquid is heated to 90 °C for 24 h under a nitrogen atmosphere. A yellow-green filter residue is obtained after filtration. The crude intermediate is dissolved in 5 mL of DMSO and refluxed for 20 min. After that, the solution is treated with 50 mL of deionized water. A yellow powder is achieved after filtration and dried under vacuum conditions. The purified product is obtained by column chromatography (neutral alumina, hexane:ethyl acetate = 5:1) as a yellow powder (0.41 g). Yield: 71%.

Pt1. ^{1}H NMR (400 MHz, DMSO-d_6): δ 8.17 (dd, J = 8.8 and 5.4 Hz, 2H), 7.98 (s, 2H), 7.90 (d, J = 7.2 Hz, 2H), 7.80 (d, J = 8.1 Hz, 2H), 7.43 (t, J = 8.8 Hz, 2H), 7.22 (t, J = 7.9 Hz, 2H), 7.11 (t, J = 7.5 Hz, 2H), 2.54 (s, 6H). ^{13}C NMR (100 MHz, DMSO-d_6): δ 163.37, 158.37, 144.20, 137.23, 130.09, 129.52, 127.78, 127.30, 127.04, 118.86, 116.38, 29.03. MALDI-TOF-MS. Calcd for $[M]$: m/z 596.09. Found: m/z 596.34. FT-IR (KBr, cm^{-1}): 3064, 2960, 2921, 1609, 1549, 1465, 1391, 1227, 773.

5. Synthesis of Pt2 (Scheme S1). A procedure similar to that for **Pt1** is used, except 4-(3,4-difluorophenyl)-2,6-diphenylpyridine (0.35 g, 1 mmol) is used in place of 4-(4-fluorophenyl)-2,6-diphenylpyr-

https://dx.doi.org/10.1021/acs.inorgchem.0c03245
Inorg. Chem. 2021, 60, 2362−2371

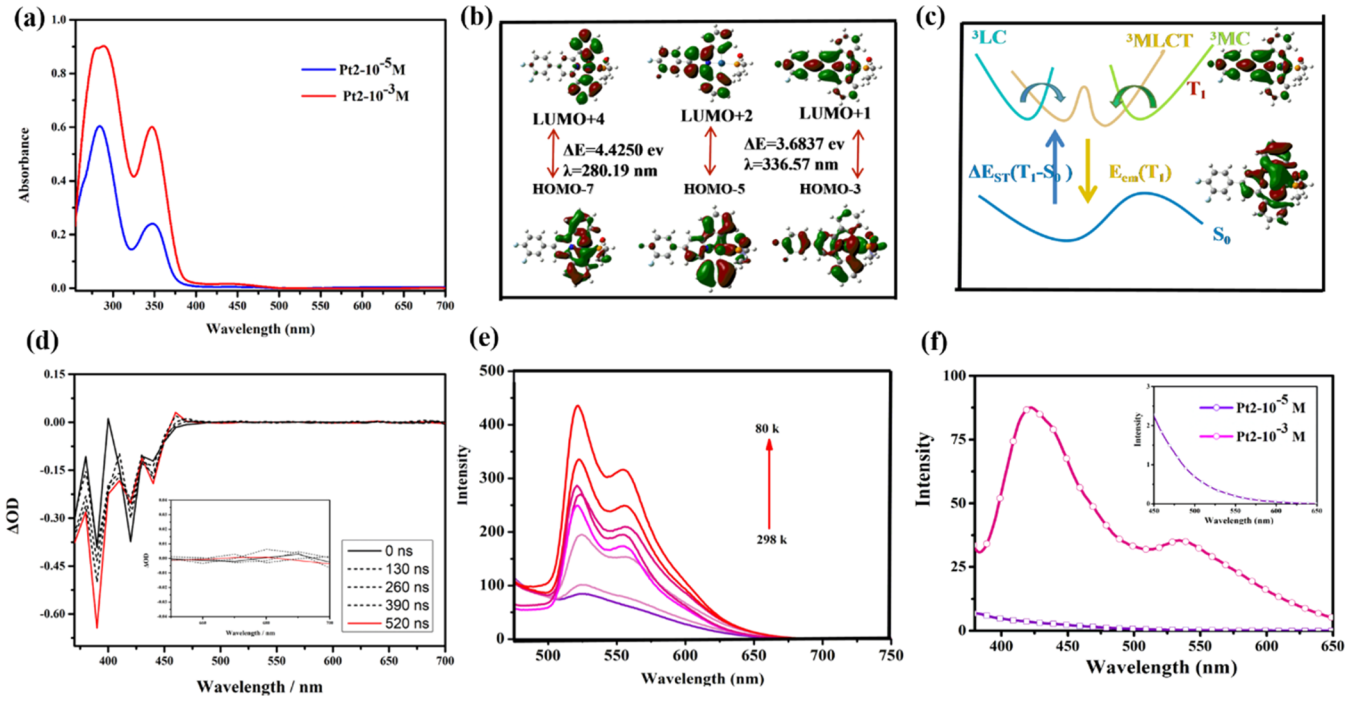

Figure 1. (a) Absorption spectra of **Pt2** (10^{-5} and 10^{-3} M). (b) Molecular orbitals of the ground and excited states of **Pt2**. (c) Schematic energy diagram showing ΔE_{ST} between the S_0 and T_1 state and relaxed T_1 state molecular orbitals. (d) TA spectra of **Pt2** (λ_{abs} = 360 nm). (e) Temperature-dependent emission spectra of a **Pt2** (10^{-3} M) complex in 2-MeTHF solutions (10^{-5} M). (f) Concentration-dependent emission spectra of **Pt2** in DMSO (10^{-5} and 10^{-3} M). Inset: Enlarged image of **Pt2** in DMSO (10^{-5} M).

idine.The final product is a yellow solid. Production: 0.39 g. Yield: 63%.

Pt2. ^{1}H NMR (400 MHz, DMSO-d_6): δ 8.31 (ddd, J = 12.2, 7.8, and 2.1 Hz, 1H), 8.02 (s, 3H), 7.92 (d, J = 7.6 Hz, 2H), 7.80 (d, J = 7.4 Hz, 2H), 7.68 (m, 1H), 7.23 (t, J = 7.3 Hz, 2H), 7.12 (t, J = 7.4 Hz, 2H), 2.54 (m, 6H). ^{13}C NMR (100 MHz, DMSO-d_6): δ 158.39, 152.37, 144.86, 138.61, 129.56, 127.63, 127.41, 127.08, 126.36, 118.08, 115.71, 29.65. MALDI-TOF-MS. Calcd for [M]: m/z 614.08. Found: m/z 614.29. FT-IR (KBr, cm^{-1}): 3050, 3002, 2921, 1606, 1539, 1250, 787.

6. Synthesis of Pt3 (Scheme S1). A procedure similar to that for **Pt1** is used, except 4-(3,5-difluorophenyl)-2,6-diphenylpyridine (0.35 g, 1 mmol) is used in place of 4-(4-fluorophenyl)-2,6-diphenylpyridine. The final product is a yellow solid. Production: 0.41 g. Yield: 67%.

Pt3. ^{1}H NMR (400 MHz, DMSO-d_6): δ 8.05 (s, 2H), 7.95 (t, J = 7.8 Hz, 4H), 7.79 (d, J = 7.8 Hz, 2H), 7.44 (t, J = 9.1 Hz, 1H), 7.23 (t, J = 7.3 Hz, 2H), 7.12 (t, J = 7.4 Hz, 2H), 2.54 (m, 6H). ^{13}C NMR (100 MHz, DMSO-d_6): δ 165.01, 158.21, 152.036, 144.61, 141.56, 129.13, 127.61, 127.28, 127.06, 118.08, 114.71, 105.90, 29.96. MALDI-TOF-MS. Calcd for [M]: m/z 614.08. Found: m/z 614.37. FT-IR (KBr, cm^{-1}): 3036, 2954, 2921, 1608, 1555, 1255, 777.

RESULTS AND DISCUSSION

Molecular Synthesis and Structure Analysis. In this study, three C^N^C cyclometalated platinum(II) complexes (**Pt1**−**Pt3**) are synthesized in a mild two-step reaction (Schemes 1a and S1). **Pt1** and **Pt2** belong to the triclinic and monoclinic systems with the P_1 and $P2_1/c$(n) space groups, respectively (Scheme 1b and Table S2). The excellent NLO response is based on the following factors: (1) Molecules with the D−A configuration give rise to ICT. (2) The introduction of DMSO and fluorine generates massive intermolecular interactions, including C−H···π (2.83 A), C−H···F (2.63 A), and C−H···O (2.69 A) interactions (Figure S18); these forces could avoid π−π stacking. (3) The central platinum coordinated with functionalized C^N^C ligands, which adopt a classical planar geometry, and the electron-withdrawing effect improve electron transfer and separation, favoring optimized NLO activity.[26,27] Further, the bond-length alternation (BLA) principle[28] could help to estimate the optical properties from the crystal data. BLA across the π bridge of **Pt1**−**Pt3** was in a reasonable range (Figure S19), indicating that these platinum(II) complexes possess a high delocalization system. Thus, the high degree of electron delocalization favors their NLO activity.

Characteristics of Singlet and Triplet States. All of the platinum(II) complexes present intense absorption bands at 280 and 340 nm (Figures 1a and S20). According to theoretical calculations (time-dependent density functional theory; Figures 1b and S21 and Table S3), the intense absorption below 300 nm for the three platinum(II) complexes could be assigned to intraligand $^1\pi,\pi^*$.[29] The moderately intense absorption around 340 nm belongs to singlet MLCT (^{1}MLCT)/singlet intraligand charge-transfer (^{1}LLCT) transitions.[30,31] On the basis of theoretical calculations (Tables S2 and S3), the possible excited-state process in platinum(II) complexes and computed T_1 states are presented in Figure 1c. Figure 1c shows the single−triplet energy gap (ΔE_{ST}) and the corresponding emission energy (E_{em}) of S_1 and T_1 of the three platinum(II) complexes. Highest occupied molecular orbital (HOMO) → lowest unoccupied molecular orbital (LUMO) is illustrated as the lowest-lying triplet state (T_1), which is attributed to the ^{3}MLCT/^{3}LLCT characteristic. The second-lowest state (T_2) is from the triplet metal-centered (^{3}MC)/^{3}MLCT characteristic and a small amount of triplet intraligand (^{3}IL), which is due to excitation centered on the ligand.[32] To investigate whether complex **Pt2** exhibits triplet excited-state absorption, the triplet transient absorption (TA) difference spectra of **Pt2** are carried out (Figure 1d). The

https://dx.doi.org/10.1021/acs.inorgchem.0c03245
Inorg. Chem. 2021, 60, 2362−2371

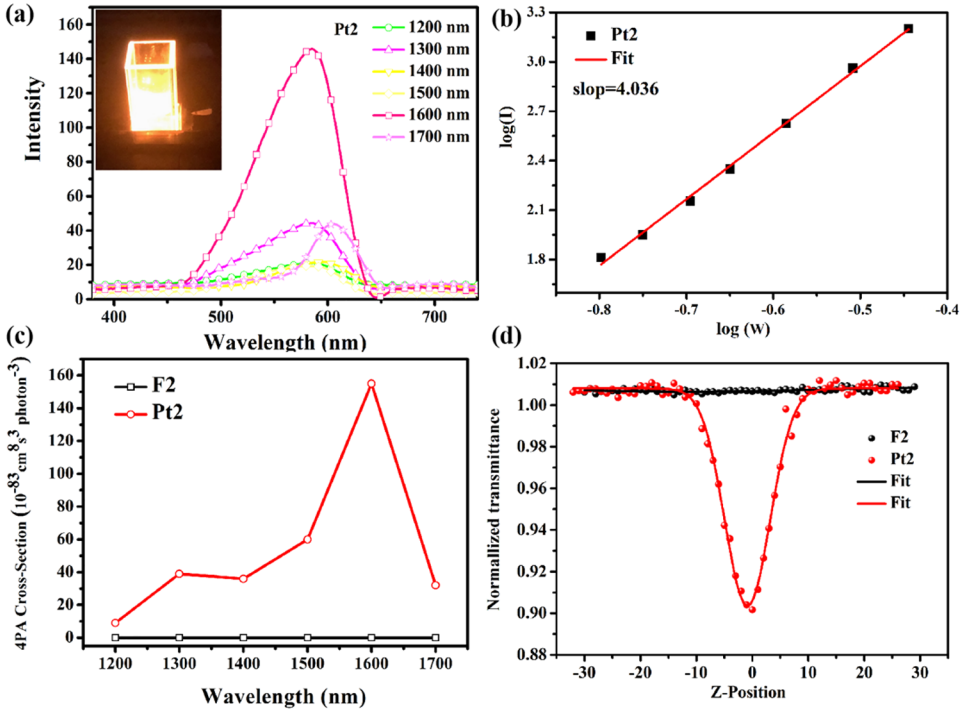

Figure 2. (a) 4PF spectra of **Pt2** under 1200−1700 nm excitation in DMSO (10^{-4} M). Inset: 4PF image of **Pt2**. (b) Fluorescence emission intensity versus incident intensity induced at a 1600 nm pump wavelength. The solid lines are the best linear fits with a slope of 4.016. (c) 4PA cross section (σ_4) of **Pt2** and **F2** under 1200−1700 nm excitation in DMSO (10^{-4} M). (d) 4PA spectra of **Pt2** and **F2** (DMSO, c = 1 mM) obtained by open-aperture Z-scan methods.

spectral features for **Pt2** have three bleaching bands between 390 and 450 nm, one relatively narrow positive band at 460 nm, and a broad moderate absorption band between 650 and 700 nm. The bleaching bands are consistent with the charge-transfer band in their UV−vis absorption. The bleaching band occurs in the region corresponding to the MLCT transition, and this feature is consistent with the excited state having MLCT character.[33] The lifetimes of **Pt2** obtained from the decay of TA are consistent with those measured from the decay of the emission (Table S4), which implies that **Pt2** probably emanates from the same excited state or in equilibrium with the emitting state. Thus, the triplet excited state shown in TA for **Pt2** is assigned to the ^{3}MLCT/^{3}LLCT excited states.[34] Most importantly, the whole spectrum is broad and positive in the NIR region, and the excited-state absorption is stronger than that of the ground state, which is present in the MLCT state.[35]

Most of the platinum(II) complexes show weak emission in a solution at room temperature.[36,37] The temperature-dependent fluorescence emission spectra are presented in Figures 1e and S23. The fluorescence intensity, quantum yields, and lifetime (Table S4) were increased, and the peak shape became more structured compared to these characteristics at room temperature. A low-temperature environment limits the molecular rotations and vibrations, which reduces the non-radiative pathways. The emission bands of **Pt1**−**Pt3** are located at 500−600 nm, and the emission peak positions are unchanged. The shoulder at 525 nm can be ascribed to a ^{3}MLCT [dπ(Pt) → π*(C^N^C)] state. The low-energy maximum at 560 nm shows a decay rate and excitation spectra similar to those at 525 nm, suggesting that this band could originate from the same excited state, namely, the ^{3}MLCT excited state.[38,39] Interestingly, Figure 1f shows that **Pt2** exhibits an obviously different concentration-dependent behavior, which is from ground-state aggregate emission.[40] The low-energy band of 540 nm corresponds to ^{3}MLCT [dπ(Pt) → π*(C^N^C)] state. According to the above, the platinum(II) complexes exhibit plentiful charge transfer and adjustable optical property, which may lead to a good NLO response and are consistent with the structural features stated.

4PA Properties. Encouraged by the reasonable and confirmable structural features and linear-optical properties above, we further investigated its NLO property. It is worth noting that research on the seven-order NLO response of those complexes has not been reported. As expected, the seven-order NLO responses of **Pt1**−**Pt3** under 1200−1700 nm (NIR region) fs laser excitation are investigated systematically. A high 4PF spectra located around 500−600 nm is observed in Figures 2a and S24a,b. The peak position showed in a red shift compared to the 1PF spectra at low temperature, and a bright yellow emission could be observed. In order to make clear the power dependence relationship of the NLO response, fluorescence emission intensity versus incident intensity was induced at a 1600 nm pump wavelength. The solid lines are the best linear fits with slope 4.03 (Figures 2b and S24c,d). The logarithms of the fluorescence intensities of **Pt1** and **Pt3** have a good linear proportion to the logarithm of the excitation power, with slopes of 4.13 and 3.91, respectively. From the above research results, we deduced that 4PF should be the main NLO process. As shown in Figure 2c, **Pt2** possesses maximum σ_4 values of up to 1.52×10^{-81} cm^8 s^3 photon^{-3}, which is larger than those of **Pt1** (0.70×10^{-81} cm^8 s^3 photon^{-3}) and **Pt3** (0.64×10^{-81} cm^8 s^3 photon^{-3}) under 1600 nm excitation (Figure S24e,f). The enhanced 4PA properties of **Pt1**−**Pt3** are confirmed further through open-aperture Z-scan methods (Figures 2d and S24g,h and Table

https://dx.doi.org/10.1021/acs.inorgchem.0c03245
Inorg. Chem. 2021, 60, 2362−2371

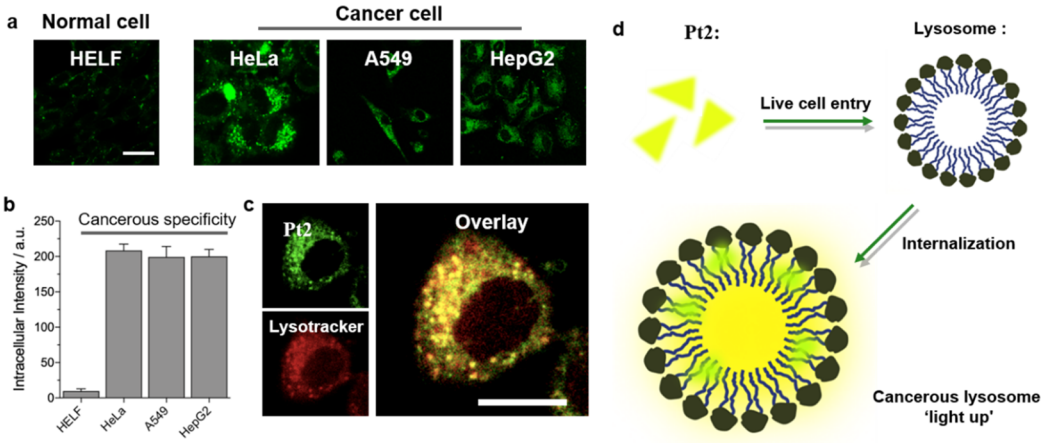

Figure 3. (a) Confocal imaging of HELF (normal) cells and HeLa, A549, and HepG2 (cancer) cells incubated with **Pt2** (10 μM, 1 h, λ_{abs} = 405 nm, λ_{em} = 480−520 nm, scale bar = 20 μm). (b) Intracellular intensity of **Pt2** incubated with **Pt2**. (c) Colocalization studies of **Pt2** with LysoTracker in HeLa cells (10 μM, 30 min, scale bar = 20 μm). (d) Schematic diagram of **Pt2** interacting with lecithin.

S5). As we expected, the 4PA properties obtained from open-aperture Z-scan measurements are consistent with the 4PF experiments. Here, we need to explain that Z-scan methods could shield energy consumed by the thermal effect and decrease the molecular rotation in the photoabsorption process, leading to a much larger 4PA cross section.

In this work, we mainly discuss the structure−activity relationship of **Pt1**−**Pt3** from the changes in the fluorine atom number, position, and primary ligand. First, fluorine has a small atomic radius, a strong electron negativity, and a similar ability to form a hydrogen bond with a hydroxyl group (−OH). These chemical properties make it easy to replace other atoms or groups with fluorine, thereby effectively adjusting the properties of the compounds.[41] In particular, the introduction of an ortho-positive fluorine atom to the conjugated chain can yield a lower HOMO energy level, rather than the meta-fluorine positions. The rigidity of the chain of ortho-position substitution was reduced. The fluorine in the ortho position was more planar than that in the meta position and closely clustered in the $\pi-\pi\pi$ direction. Therefore, good chain planarity could increase light absorption and improve charge transfer.[42] As a result, the fluorine atom on the C^N cyclometalating groups results in an increase in the 4PA cross section, which shows the tendency **Pt1** < **Pt3** < **Pt2**.

Second, compared to 2,2′-bipyridine and terpyridine complexes (N^N and N^N^N), the platinum(II) complexes with tridentate pincer ligands (C^N^C and N^C^N) could further raise the energy of the d−d excited states and effectively reduce the probability of nonradiative pathways in the nonemission ligand-field state because of their stronger σ-donating effect.[43] The introduction of a Pt−C bond makes the complexes possess more stable and better properties. Therefore, **Pt2** coordinated by a tridentate C^N^C ligand shows high thermal/photostability as well as remarkable multiphoton activities in the NIR region.

Further, we also discuss a comparison of the 4PA cross section between **Pt1**−**Pt3** and some reported cases in the organic counterparts. Hernández et al. illustrate that the 4PA cross section of (7-benzothiazol-2-yl-9,9-didecylfluoren-2-yl)-diphenylamine is 8.1 × 10^{-109} cm^8 s^3 $photon^{-3}$.[44] Simpson et al. reported the syntheses of three aryleneethynylene-based organic dendrimers, with the ruthenated dendrimer Ru9 exhibiting significant 4PA behavior (2100 × 10^{-110} cm^8 s^3 at 1600 nm) under 1600 nm excitation.[45] The reported 4PA cross sections of the organic molecules are far smaller than what we demonstrated.

All of the results stated above showed that the 4PA property will motivate the platinum(II) complexes to be employed as 4PF probes in disease diagnosis and treatment.

Anticancer Therapy. In our previous work, we designed and synthesized a neutral cyclometalated platinum complex that has been confirmed to inhibit NF-κB gene transcription. Interestingly, the platinum(II) complex can upregulate the nuclear translocation of cancer cells rather than normal cells, thereby inhibiting the proliferation of cancer cells without interfering with healthy cells. Therefore, compared to traditional platinum complexes, the Pt−C bond has higher persistence in the biological environment and less toxicity to heavy metals, which may distinguish cancer cells from normal cells.[46,47] Further, the toxicity of the platinum(II) complex can be reduced by inserting an S-donor molecule of DMSO into the platinum(II) coordination sphere; on the other hand, as a labeling ligand, DMSO could reduce the toxicity, increase the water solubility (Figure S25), and enhance the anticancer activity in vitro.[48]

The biggest drawbacks of the traditional anticancer drug (cisplatin) are its inability to distinguish between normal cells and cancer cells effectively and its high toxicity for normal cells.[49−52] In contrast to the above defects, we attempt to use **Pt1**−**Pt3** to visually distinguish between human embryo liver fibroblast (HELF) cells and three kinds of cancer cells under confocal imaging. According to confocal imaging (Figures S26 and 3a,b), **Pt1**−**Pt3** shows weak fluorescence signals in the HELF cells but obvious fluorescence signals in HeLa, A549, and HePG2 cells. Further, **Pt2** shows strong colocalization to lysosome in HeLa cells (Figures S27 and 3c). The possible lysosome-targeting mechanisms are shown in Figure 3d. Lysosomes are the key targets for therapeutic intervention in neurodegenerative disorders and cancer, and lysosomes could induce apoptosis. According to several studies, the high dependence on the lysosome pathway and the decrease of the lysosome stability in cancer cells make lysosome a particularly suitable choice as an anticancer drug because cancer cells are more prone to drug-induced lysosomal instability than normal tissues.[53]

https://dx.doi.org/10.1021/acs.inorgchem.0c03245
Inorg. Chem. 2021, 60, 2362−2371

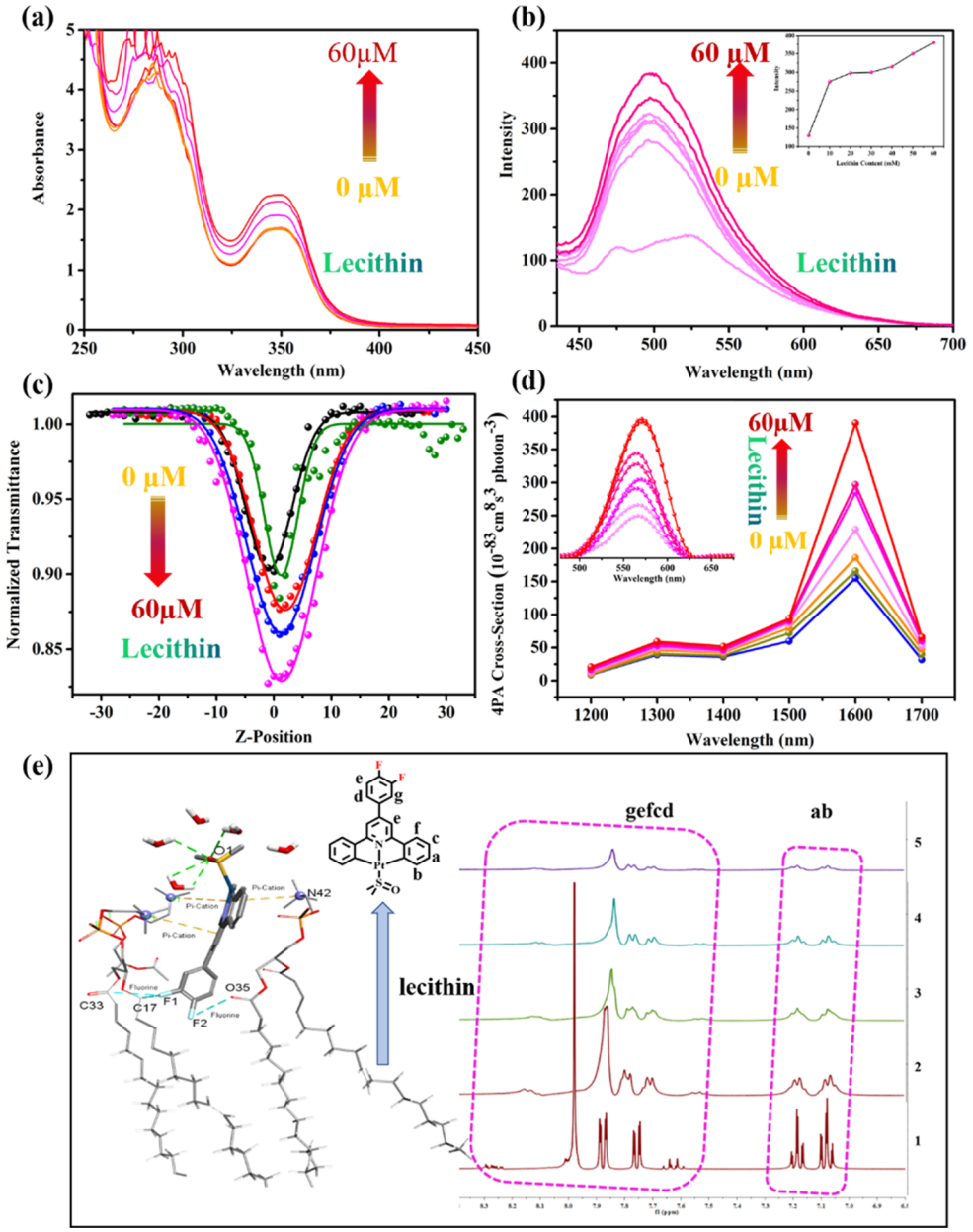

Figure 4. (a and b) UV−vis absorption and fluorescence intensity of **Pt2** (10^{-3} M) in the presence of amounts of lecithin (0−60 μM, Tris-HCl buffer, pH = 7.4). (c) 4PA spectra of **Pt2** obtained under various amounts of lecithin (0−60 μM). (d) Four-photon (TP) action cross section of **Pt2** under various amounts of lecithin (0−60 μM). Inset: 4PF changes under various amounts of lecithin (0−60 μM). (e) (Left) Intramolecular interaction between the platinum complex and lecithin. (Right) ^{1}H NMR titration spectra for **Pt2** + lecithin in D_2O.

As is known, lecithin is the essential component of membranes because it plays an important physiological role in lysosome.[54] To obtain more insight into how **Pt2** targets lysosome, lecithin as the main component of the lysosomal membrane was screened in vitro. Obviously, **Pt2** shows a distinct response to lecithin (Figure S28). The absorption titration studies (Figure 4a) were carried out using a fixed concentration of **Pt2** and an increasing amount of lecithin. The extent of hyperchromism (46%) upon the addition of lecithin indicates that **Pt2** interacts with lecithin through electrostatic interaction (Figure S29). To compare their lecithin binding affinity, the intrinsic binding constant K_b was calculated;[55] as usual the value of K_b is 1.013×10^7. The fluorescence intensity of **Pt2** (Figure 4b) increased 5-fold compared to that in pure **Pt2**. The 4PA properties of **Pt2** with lecithin were also measured by both 4PF and open-aperture Z scanning (Figure 4c,d). The 4PA cross section of **Pt2** was increased about 2.6-fold (3.9×10^{-81} cm^8 s^3 photon^{-3}) after 60 μM lecithin was added (Figures 4c,d and S31). Molecular docking techniques are valuable for understanding the weak interaction about the van der Waals and hydrogen-bonding interactions (Figure 4e, left).[46,56] We studied the binding ability between **Pt2** and lecithin by using *Discovery Studio 4.1*. The **Pt2** ligand is set in the lecithin polar group layer, and in the **Pt2** molecule, the carbonyl oxygen atom (O1) on DMSO forms a hydrogen bond with water molecules. The benzene and pyridine rings and cationic nitrogen atom of the lecithin molecules form multiple π−cation interactions, and the interaction between the fluorine atoms (F1 and F2) in the benzene ring and ester oxygen atom (O35) and carbonyl carbon atoms (C17 and C33) in the

https://dx.doi.org/10.1021/acs.inorgchem.0c03245
Inorg. Chem. 2021, 60, 2362−2371

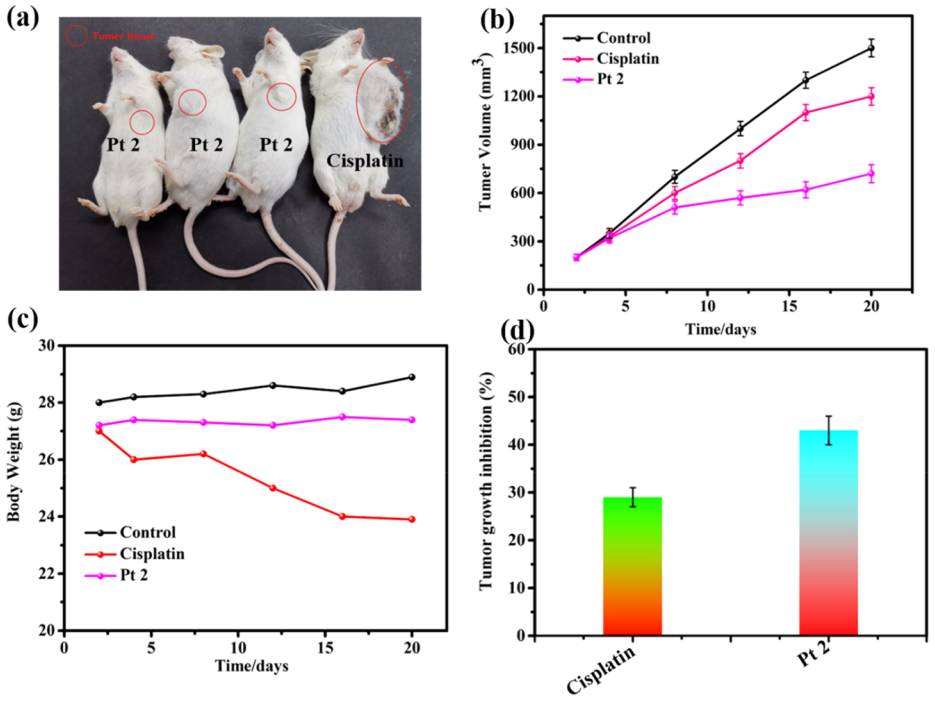

Figure 5. (a) Gross morphology of mice after intratumor injection with **Pt2** and cisplatin at 20th day. (b) Tumor volumes of the mice model over 20 days. (c) Tumor growth inhibition rate with **Pt2** and cisplatin treatment over 20 days. (d) Mice body weight over 20 days.

lecithin molecule is a halogen atom interaction. Figure 4e (right) shows that the proton signals $H_a \sim H_g$ on the pyridine and benzene rings moved toward high magnetic fields after lecithin addition, and the intensity decreased gradually, indicating that the hydrogen atoms in those locations may bind with lecithin. Meanwhile, density functional theory calculation (Figure S32) also shows the high electron density on the pyridine and benzene rings when interacting with lecithin.

Considering the above results, we tentatively suggest that **Pt2** could target lysosome because of interaction with lecithin on the lysosomal membrane. So, **Pt2** is promising as a four-photon biological probe to recognize cancer cells under the NIR window (1600 nm) in cancer theranostics.

Despite the excellent specificity identification of **Pt2** to cancer cells, the high side effects of damage to normal cells should not be ignored. According to MTT results (Figure S33), **Pt2** shows high cytotoxicity to HeLa cells (IC_{50} = 0.63 μM) and negligible cytotoxicity to HELF cells. In contrast, cisplatin showed an obvious low toxicity (IC_{50} = 1.99 μM) to HeLa cancer cells and higher toxicity to normal cells than platinum complexes. As indicated above, it is strongly suggested that **Pt2** could selectively damage cancer cells in vitro. Thus, we further explored the therapeutic effect of **Pt2** in vivo (Figure 5). The results showed that the mice tumor treated with cisplatin still grew in volume, accompanied by ulceration of the skin. However, the mice tumor treated with **Pt1**−**Pt3** complexes showed negligible gross changes in the tumor volume (Figure 5a−c). Further, the body weight of the **Pt1**−**Pt3**-treated mice remains similar to that of the PBS-treated mice, while a decreasing tendency was observed in the cisplatin treatment (Figure 5d). The ex vivo image (Figure S34) showed that **Pt2** was mostly focused on liver and negligibly focused on kidney, spleen, and lung. **Pt2** is thus proven to be a potential cancer therapy agent, making it an attractive chemotherapeutic agent, with a better therapeutic index and a lower toxicity toward normal tissues.

CONCLUSIONS

In summary, we have presented herein the first 4PA C^N^C cyclometalated platinum(II) complexes for cancer theranostics. Structural evidence reveals that platinum(II) complexes impose little steric hindrance and moderate BLA favoring their NLO activity. These complexes are stable in solution and exhibit broad excited-state absorption (^{3}MLCT) characteristics. According to the investigation under four-photon excitation, **Pt2** possesses an excellent 4PA cross section of 1.52×10^{-81} cm^8 s^3 photon^{-3} visible-to-NIR region excitation. Moreover, it is apparent that **Pt2** shows high toxicity to cancer cells and a fluorescence-staining pattern of lysosome due to interaction with lecithin. Anticancer therapy on the mouse model also shows that **Pt2** presents excellent anticancer activity. We believe that designing functionalized 4PA platinum(II) complexes will have a potential application in anticancer treatment to achieve better biocompatibility and cancer therapy.

ASSOCIATED CONTENT

Supporting Information

The Supporting Information is available free of charge at https://pubs.acs.org/doi/10.1021/acs.inorgchem.0c03245.

Additional experimental data including synthesis procedures, characterization data, photophysical properties, and experimental details (PDF)

Accession Codes

CCDC 1876585, 1876670, 1876757, 1876787, 1941434, and 1970263 contain the supplementary crystallographic data for this paper. These data can be obtained free of charge via www.ccdc.cam.ac.uk/data_request/cif, or by emailing data_request@ccdc.cam.ac.uk, or by contacting The Cambridge

https://dx.doi.org/10.1021/acs.inorgchem.0c03245
Inorg. Chem. 2021, 60, 2362−2371

Crystallographic Data Centre, 12 Union Road, Cambridge CB2 1EZ, UK; fax: +44 1223 336033.

AUTHOR INFORMATION

Corresponding Authors

Qiong Zhang − *Department of Chemistry, Key Laboratory of Functional Inorganic Material Chemistry of Anhui Province, Anhui University, Hefei 230601, P. R. China;* orcid.org/0000-0002-5360-3951; Email: zhangqiong.314@163.com

Xiaohe Tian − *School of Life Science, Anhui University, Hefei 230601, P. R. China;* orcid.org/0000-0002-2294-3945; Email: xiaohe.t@ahu.edu.cn

Yupeng Tian − *Department of Chemistry, Key Laboratory of Functional Inorganic Material Chemistry of Anhui Province, Anhui University, Hefei 230601, P. R. China;* Email: yptian@ahu.edu.cn

Authors

Shujing Wang − *Department of Chemistry, Key Laboratory of Functional Inorganic Material Chemistry of Anhui Province, Anhui University, Hefei 230601, P. R. China*

Yingzhong Zhu − *Department of Chemistry, Key Laboratory of Functional Inorganic Material Chemistry of Anhui Province, Anhui University, Hefei 230601, P. R. China*

Chengkai Zhang − *Department of Chemistry, Key Laboratory of Functional Inorganic Material Chemistry of Anhui Province, Anhui University, Hefei 230601, P. R. China*

Hongzhi Cao − *School of Life Science, Anhui University, Hefei 230601, P. R. China*

Wen Ma − *Department of Chemistry, Key Laboratory of Functional Inorganic Material Chemistry of Anhui Province, Anhui University, Hefei 230601, P. R. China*

Jieying Wu − *Department of Chemistry, Key Laboratory of Functional Inorganic Material Chemistry of Anhui Province, Anhui University, Hefei 230601, P. R. China*

Hongping Zhou − *Department of Chemistry, Key Laboratory of Functional Inorganic Material Chemistry of Anhui Province, Anhui University, Hefei 230601, P. R. China;* orcid.org/0000-0003-3502-6836

Complete contact information is available at: https://pubs.acs.org/10.1021/acs.inorgchem.0c03245

Author Contributions

†Q.Z. and S.J.W. contributed equally to this work.

Notes

The authors declare no competing financial interest.

ACKNOWLEDGMENTS

This work was financially supported by the National Natural Science Foundation of China (Grants 21871003, 51672002, 21701160, 21602003, and 51772002), Start-up Grant from Anhui University (Grants S020118002/073 and S020118002/026), and Anhui Provincial Natural Science Foundation of China (Grants 1708085MC68 and 1908085MB30).

REFERENCES

(1) Elhussin, I.; Zhang, S.; Liu, J.; Li, D.; Zhang, Q.; Li, S.; Tian, X.; Wu, J.; Tian, Y. A novel water-soluble quinoline−indole derivative as a three-photon fluorescent probe for identifying nucleolus RNA and mitochondrial DNA. *Chem. Commun.* **2020**, *56*, 1859−1862.

(2) Zhang, R.; Niu, G.; Lu, Q.; Huang, X.; Chau, J.; Kwok, R.; Yu, X.; Li, M.; Lam, J.; Tang, B. Cancer cell discrimination and dynamic viability monitoring through wash-free bioimaging using AIEgens. *Chem. Sci.* **2020**, *11*, 7676−7684.

(3) Cheng, X.; Yang, F.; Zhao, J.; Ni, J.; He, X.; Zhou, C.; Sun, J.; Tang, B. Microscopic visualization and mechanism investigation of the crystal jumping behavior of a cyclic chalcone derivative. *Mater. Chem. Front.* **2020**, *4*, 651−660.

(4) Manzi, A.; Tong, Y.; Feucht, J.; Yao, E.; Polavarapu, L.; Urban, A.; Feldmann, J. Resonantly enhanced multiple exciton generation through below-band-gap multi-photon absorption in perovskite nanocrystals. *Nat. Commun.* **2018**, *9*, 1518.

(5) Chen, C.; Wang, F.; Wen, S.; Su, Q.; Wu, M.; Liu, Y.; Wang, B.; Li, D.; Shan, X.; Kianinia, M.; Aharonovich, I.; Toth, L.; Jackson, S.; Xi, P.; Jin, D. Multi-photon near-infrared emission saturation nanoscopy using upconversion nanoparticles. *Nat. Commun.* **2018**, *9*, 3290.

(6) Das, B.; Shi, L.; Budansky, Y.; Rodriguez-Contreras, A.; Alfano, R. Alzheimer mouse brain tissue measured by time resolved fluorescence spectroscopy using single- and multi-photon excitation of label free native molecules. *J. Biophotonics.* **2018**, *11*, e201600318.

(7) Li, R.; Dong, N.; Ren, F.; Amekura, H.; Wang, J.; Chen, F. Nonlinear Absorption Response Correlated to Embedded Ag Nanoparticles in BGO Single Crystal: From Two-Photon to Three-Photon Absorption. *Sci. Rep.* **2018**, *8*, 1977.

(8) Wang, Y.; Han, X.; Xi, W.; Li, J.; Roe, A.; Lu, P.; Qian, J. Bright AIE Nanoparticles with F127 Encapsulation for Deep-Tissue Three-Photon Intravital Brain Angiography. *Adv. Healthcare Mater.* **2017**, *6*, 1700685−1700695.

(9) Ohta, S.; Nakano, M.; Kubo, T.; Kamada, K.; Ohta, K.; Kishi, R.; Nakagawa, N.; et al. Theoretical Study on the Second Hyperpolarizabilities of Phenalenyl Radical Systems Involving Acetylene and Vinylene Linkers: Diradical Character and Spin Multiplicity Dependences. *J. Phys. Chem. A* **2007**, *111*, 3633−3641.

(10) Liu, W.; Wang, Y.; Han, X.; Lu, P.; Zhu, L.; Sun, C.; Qian, J.; He, S. Fluorescence resonance energy transfer (FRET) based nanoparticles composed of AIE luminogens and NIR dyes with enhanced three-photon near-infrared emission for in vivo brain angiography. *Nanoscale* **2018**, *10*, 10025−10032.

(11) Wu, P.; Feng, X.; Tam, H.; Wong, M.; Cheah, K. Efficient Three-Photon Excited Deep Blue Photoluminescence and Lasing of Diphenylamino and 1,2,4-Triazole Endcapped Oligofluorenes. *J. Am. Chem. Soc.* **2009**, *131*, 886−887.

(12) Gong, P.; Liang, F.; Kang, L.; Chen, X.; Qin, J.; Wu, Y.; Lin, Z. Recent advances and future perspectives on infrared nonlinear optical metal halides. *Coord. Chem. Rev.* **2019**, *380*, 83−102.

(13) Gu, B.; Zhao, C.; Baev, A.; Yong, K.-T.; Wen, S.; Prasad, P. Molecular nonlinear optics: recent advances and applications. *Adv. Opt. Photonics* **2016**, *8*, 328−369.

(14) Shao, P.; Li, Y.; Azenkeng, A.; Hoffmann, M.; Sun, W. Influence of Alkoxyl Substituent on 4,6-Diphenyl-2,2′-bipyridine Ligand on Photophysics of Cyclometalated Platinum(II) Complexes: Admixing Intraligand Charge Transfer Character in Low-Lying Excited States. *Inorg. Chem.* **2009**, *48*, 2407−2419.

(15) Shao, P.; Li, Y.; Yi, J.; Pritchett, T.; Sun, W. Cyclometalated Platinum(II) 6-Phenyl-4-(9,9-dihexylfluoren-2-yl)-2,2′-bipyridine Complexes: Synthesis, Photophysics, and Nonlinear Absorption. *Inorg. Chem.* **2010**, *49*, 4507−4517.

(16) Rogers, J.; Slagle, J.; Krein, D.; Burke, A.; Hall, B.; Fratini, A.; McLean, D. G.; Fleitz, P. A.; Cooper, T. M.; Drobizhev, M.; Makarov, N.; Rebane, A.; Kim, K.; Farley, R.; Schanze, K. Platinum Acetylide Two-Photon Chromophores. *Inorg. Chem.* **2007**, *46*, 6483−6494.

(17) Liu, R.; Hu, J.; Zhu, S.; Lu, J.; Zhu, H. Synergistically Enhanced Optical Limiting Property of Graphene Oxide Hybrid Materials Functionalized with Pt Complexes. *ACS Appl. Mater. Interfaces* **2017**, *9*, 33029−3040.

(18) Coe, B. Developing iron and ruthenium complexes for potential nonlinear optical applications. *Coord. Chem. Rev.* **2013**, *257*, 1438−1458.

(19) Johnstone, T.; Suntharalingam, K.; Lippard, S. The Next Generation of Platinum Drugs: Targeted Pt(II) Agents, Nanoparticle Delivery, and Pt(IV) Prodrugs. *Chem. Rev.* **2016**, *116*, 3436−3486.
(20) Legin, A.; Theiner, S.; Schintlmeister, A.; Reipert, S.; Heffeter, P.; Jakupec, M.; Mayr, J.; Varbanov, H.; Kowol, C.; Galanski, M.; Berger, W.; Wagner, M.; Keppler, B. K. Multi-scale imaging of anticancer platinum(iv) compounds in murine tumor and kidney. *Chem. Sci.* **2016**, *7*, 3052−3061.
(21) Anulewicz, R.; Bak, T.; Cyranski, M.; Krygowski, T.; Rasala, D.; Swirska, B. Substituent Effect on Geometry of the Pyridine and Benzene Rings in Some 4-Aryl-2,6-Diphenylpyridines—Crystal and Molecular-Structure of Methyl and Fluoro Derivatives. *Polym. J. Chem.* **1995**, *69*, 597−604.
(22) Garbe, S.; Krause, M.; Klimpel, A.; Neundorf, I.; Lippmann, P.; Ott, I.; Brunink, D.; Strassert, C.; Doltsinis, N.; Klein, A. Cyclometalated Pt Complexes of CNC Pincer Ligands: Luminescence and Cytotoxic Evaluation. *Organometallics* **2020**, *39*, 746.
(23) Censi, V.; Caballero, A.; Pérez-Hernández, M.; Soto-Cerrato, V.; Korrodi-Gregório, L.; Pérez-Tomás, R.; Dell'Anna, M.; Mastrorilli, P.; Gamez, P. DNA-binding and in vitro cytotoxic activity of platinum(II) complexes of curcumin and caffeine. *J. Inorg. Biochem.* **2019**, *198*, 110749.
(24) Gill, M.; Vallis, K. Transition metal compounds as cancer radiosensitizers. *Chem. Soc. Rev.* **2019**, *48*, 540−557.
(25) Kenny, R.; Marmion, C. Toward Multi-Targeted Platinum and Ruthenium Drugs—A New Paradigm in Cancer Drug Treatment Regimens? *Chem. Rev.* **2019**, *119*, 1058−1137.
(26) Sicilia, V.; Fornies, J.; Casas, J.; Martín, A.; López, J.; Larraz, C.; Borja, P.; Ovejero, C.; Tordera, D.; Bolink, H. Highly Luminescent Half-Lantern Cyclometalated Platinum(II) Complex: Synthesis, Structure, Luminescence Studies, and Reactivity. *Inorg. Chem.* **2012**, *51*, 3427−3435.
(27) Fang, B.; Zhu, Y.; Hu, L.; Shen, Y.; Jiang, G.; Zhang, Q.; Tian, X.; Li, S.; Zhou, H.; Wu, J.; Tian, Y. Series of C∧N∧C Cyclometalated Pt(II) Complexes: Synthesis, Crystal Structures, and Nonlinear Optical Properties in the Near-Infrared Region. *Inorg. Chem.* **2018**, *57*, 14134−14143.
(28) Marder, S.; Gorman, C.; Tiemann, B.; Perry, J.; Bourhill, G.; Mansour, K. Relation Between Bond-Length Alternation and Second Electronic Hyperpolarizability of Conjugated Organic Molecules. *Science* **1993**, *261*, 186−189.
(29) Fuertes, S.; Brayshaw, S.; Raithby, P.; Schiffers, S.; Warren, M. New C∧N∧N Bis-Cyclometalated Platinum(II) Complexes: Synthesis, Structures, and Photophysical Properties. *Organometallics* **2012**, *31*, 105−119.
(30) Guo, F.; Sun, W. Photophysics and Optical Limiting of Platinum(II) 4′-Arylterpyridyl Phenylacetylide Complexes. *J. Phys. Chem. B* **2006**, *110*, 15029−15036.
(31) Ohno, K.; Hasebe, M.; Nagasawa, A.; Fujihara, T. Change in Luminescence Induced by Solution-Mediated Phase-Transition of Cyclometalated Platinum(II) Complex with Isoquinoline Carboxylate. *Inorg. Chem.* **2017**, *56*, 12158−12168.
(32) Kong, F.; Tang, M.; Wong, Y.; Ng, M.; Chan, M.; Yam, V. Strategy for the Realization of Efficient Solution-Processable Phosphorescent Organic Light-Emitting Devices: Design and Synthesis of Bipolar Alkynylplatinum(II) Complexes. *J. Am. Chem. Soc.* **2017**, *139*, 6351−6362.
(33) Guo, F.; Sun, W.; Liu, Y.; Schanze, K. Synthesis, Photophysics, and Optical Limiting of Platinum(II) 4′-Tolylterpyridyl Arylacetylide Complexes. *Inorg. Chem.* **2005**, *44*, 4055−4065.
(34) Liu, R.; Chen, H.; Chang, J.; Li, Y.; Zhu, H.; Sun, W. Pt(ii) diimine complexes bearing carbazolyl-capped acetylide ligands: synthesis, tunable photophysics and nonlinear absorption. *Dalton Trans.* **2013**, *42*, 160−171.
(35) Whittle, C.; Weinstein, J.; George, M.; Schanze, K. Photophysics of Diimine Platinum(II) Bis-Acetylide Complexes. *Inorg. Chem.* **2001**, *40*, 4053−4062.
(36) Díez, A.; Forniés, J.; Larraz, C.; Lalinde, E.; López, J.; Martín, A.; Sicilia, V.; Moreno, M. Structural and Luminescence Studies on $\pi\cdots\pi$ and Pt···Pt Interactions in Mixed Chloro-Isocyanide Cyclometalated Platinum(II) Complexes. *Inorg. Chem.* **2010**, *49*, 3239−3251.
(37) Ohno, K.; Hasebe, M.; Nagasawa, A.; Fujihara, T. Change in Luminescence Induced by Solution-Mediated Phase-Transition of Cyclometalated Platinum(II) Complex with Isoquinoline Carboxylate. *Inorg. Chem.* **2017**, *56*, 12158−12168.
(38) Liu, B.; Lystrom, L.; Kilina, S.; Sun, W. Effects of Varying the Benzannulation Site and π Conjugation of the Cyclometalating Ligand on the Photophysics and Reverse Saturable Absorption of Monocationic Iridium(III) Complexes. *Inorg. Chem.* **2019**, *58*, 476−488.
(39) Tam, A.; Lam, W.; Wong, K.; Zhu, N.; Yam, V. Luminescent Alkynylplatinum(II) Complexes of 2,6-Bis(N-alkylbenzimidazol-2′-yl)pyridine-Type Ligands with Ready Tunability of the Nature of the Emissive States by Solvent and Electronic Property Modulation. *Chem. - Eur. J.* **2008**, *14*, 4562−4576.
(40) Li, Z.; Sun, W. Synthesis, photophysics, and reverse saturable absorption of platinum complexes bearing extended π-conjugated C∧N∧N ligands. *Dalton Trans.* **2013**, *42*, 14021−14029.
(41) Chen, Y.; Liu, C.; Wang, L. Effects of fluorine substituent on properties of cyclometalated iridium(III) complexes with a 2,20-bipyridine ancillary ligand. *Tetrahedron* **2019**, *75*, 130686.
(42) Shin, J.; Kim, M.; Lee, J.; Kim, H.; Hwang, H.; Cho, K. Positional effects of fluorination in conjugated side chains on photovoltaic properties of donor−acceptor copolymers. *Chem. Commun.* **2017**, *53*, 1176−1179.
(43) Ai, Y.; Li, Y.; Ma, H.; Su, C.; Yam, V. Cyclometalated Platinum(II) Complexes of 1,3-Bis(1-n-butylpyrazol-3-yl)benzenes: Synthesis, Characterization, Electrochemical, Photophysical, and Gelation Behavior Studies. *Inorg. Chem.* **2016**, *55*, 11920−11929.
(44) Hernández, F.; Belfield, K.; Cohanoschi, I.; Balu, M.; Schafer, K. Three- and four-photon absorption of a multiphoton absorbing fluorescent probe. *Appl. Opt.* **2004**, *43*, 5394−5398.
(45) Simpson, P.; Watson, L.; Barlow, A.; Wang, G.; Cifuentes, M.; Humphrey, M. Record Multiphoton Absorption Cross-Sections by Dendrimer Organometalation. *Angew. Chem.* **2016**, *128*, 2433−2437.
(46) Zhu, Y.; Zhang, M.; Luo, L.; Gill, M.; De Pace, C.; Battaglia, G.; Zhang, Q.; Zhou, H.; Wu, J.; Tian, Y.; Tian, X. NF-κB hijacking theranostic Pt(ll) complex in cancer therapy. *Theranostics* **2019**, *9*, 2158−2166.
(47) Liu, J.; Sun, R.; Leung, C.; Lok, C.; Che, C. Inhibition of TNF-α stimulated nuclear factor-kappa B (NF-κB) activation by cyclometalated platinum (II) complexes. *Chem. Commun.* **2012**, *48*, 230−232.
(48) Jakubowski, M.; Łakomska, I.; Sitkowski, J.; Wiśniewska, J. Dicarboxylato platinum(II) complexes containing dimethyl sulfoxide and triazolopyrimidine as potential anticancer agents: synthesis, structural and biological studies in solution. *New J. Chem.* **2018**, *42*, 8113.
(49) Sancho-Martínez, S.; Prieto-García, L.; Prieto, M.; Lopez-Novoa, J.; López-Hernández, F. Subcellular targets of cisplatin cytotoxicity: An integrated view. *Pharmacol. Ther.* **2012**, *136*, 35−55.
(50) Köberle, B.; Tomicic, M.; Usanova, S.; Kaina, B. Cisplatin resistance: Preclinical findings and clinical implications. *Biochim. Biophys. Acta, Rev. Cancer* **2010**, *1806*, 172−182.
(51) Kelland, L. The resurgence of platinum-based cancer chemotherapy. *Nat. Rev. Cancer* **2007**, *7*, 573−584.
(52) Kuo, W.-Y.; Hwu, L.; Wu, C.-Y.; Lee, J.-S.; Chang, C.-W.; Liu, R.-S. STAT3/NF-κB-Regulated Lentiviral TK/GCV Suicide Gene Therapy for Cisplatin-Resistant Triple-Negative Breast Cancer. *Theranostics* **2017**, *7*, 647−663.
(53) Tegeder, I.; Kogel, D. When lipid homeostasis runs havoc: lipotoxicity links lysosomal dysfunction to autophagy. *Matrix Biol.* **2020** DOI: 10.1016/j.matbio.2020.11.005.
(54) Bai, X.; Xu, Lu; Tang, J.; Zuo, Y.; Hu, G. Adsorption of Phospholipids at the Air-Water Surface. *Biophys. J.* **2019**, *117*, 1224−1233.

(55) Paitandi, R.; Mukhopadhyay, S.; Singh, R.; Sharma, V.; Mobin, S.; Pandey, D. Anticancer Activity of Iridium(III) Complexes Based on a PyrazoleAppended Quinoline-Based BODIPY. *Inorg. Chem.* **2017**, *56*, 12232−12247.
(56) Feng, Z.; Li, D.; Zhang, M.; Shao, T.; Shen, Y.; Tian, X.; Zhang, Q.; Li, S.; Wu, J.; Tian, Y. Enhanced three-photon activity triggered by the AIE behaviour of a novel terpyridine-based Zn(II) complex bearing a thiophene bridge. *Chem. Sci.* **2019**, *10*, 7228.

https://dx.doi.org/10.1021/acs.inorgchem.0c03245
Inorg. Chem. 2021, 60, 2362−2371